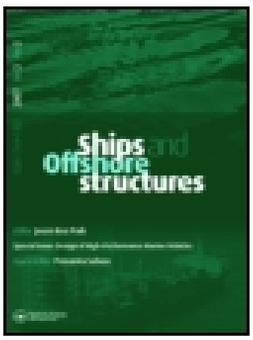

Taylor & Francis
Taylor & Francis Group

Ships and Offshore Structures

ISSN: (Print) (Online) Journal homepage: https://www.tandfonline.com/loi/tsos20

Coupling of dynamic reaction forces of a heavy load crane and ship motion responses in waves

Yingguang Chu, Guoyuan Li, Lars Ivar Hatledal, Finn Tore Holmeset & Houxiang Zhang

To cite this article: Yingguang Chu, Guoyuan Li, Lars Ivar Hatledal, Finn Tore Holmeset & Houxiang Zhang (2021): Coupling of dynamic reaction forces of a heavy load crane and ship motion responses in waves, Ships and Offshore Structures, DOI: 10.1080/17445302.2021.1907066

To link to this article: https://doi.org/10.1080/17445302.2021.1907066

Published online: 10 Apr 2021.

SHIPS AND OFFSHORE STRUCTURES
https://doi.org/10.1080/17445302.2021.1907066

Taylor & Francis
Taylor & Francis Group

Coupling of dynamic reaction forces of a heavy load crane and ship motion responses in waves

Yingguang Chu [a], Guoyuan Li [b], Lars Ivar Hatledal[b], Finn Tore Holmeset[b] and Houxiang Zhang [b]

[a]Sintef Ålesund AS Ålesund, Norway; [b]Department of Ocean Operations and Civil Engineering, Faculty of Engineering, Norwegian University of Science and Technology Ålesund, Norway

ABSTRACT

The conventional approach to dynamic analysis of ship motion response with shipboard operation equipment is usually done by establishing combined equations of motion of the multi-body system. The weakness of such methods is usually associated with the effectiveness of modelling and the simulation efficiency of computing the dynamic ship responses in waves in the time domain. In recent years, time domain simulation of nonlinear ship motion response in waves has become more and more popular. In this paper, we present coupled simulation of a heavy load crane with interactive ship motion responses in waves. The static gravitational forces of the crane system and dynamic excitation forces from the payload are applied to the ship as external forces on varying attack points of the hull during crane operations. Simulation of the crane operation is implemented in the digital twin ship platform and demonstrated meaningful physical behaviours.

ARTICLE HISTORY
Received 27 October 2020
Accepted 7 March 2021

KEYWORDS
Ship motion response; crane operation; co-simulation; tight-coupling; multi-body dynamics

1. Introduction

Cranes are important deck equipment in many offshore and subsea applications for lifting, transferring and handling objects and personnel. Unlike land-based cranes on fixed working platforms, maritime crane operations are affected by the ship motion in waves and the suspended load, and vice versa. Due to these inherent issues such as heavy lifting, positioning accuracy, load sway and security, maritime crane operations are demanding tasks in terms of both work efficiency and safety. Especially, large ship motions can be induced by external disturbances from heavy loading conditions in rough weather environment. Figure 1 shows a typical offshore crane in subsea installation on the small research vessel Gunnerus.

Usually, dynamic modelling and simulation of multi-body system operations are carried out independent of the hydrodynamic interactions to the ship. For example, the dynamic coupling between crane, including the payload, and ship motion was studied for a floating crane barge (Schellin et al. 1991). This approach has proven to be acceptable based on studies carried out for crane-ship coupled motions. It is shown that the hydrodynamic interaction effects are an order of magnitude smaller than the mechanical coupling effects, i.e. the coupling between the crane and the ship (Baar et al. 1992). Alternatively, coupled modelling of the ship and crane can be established by combined equations of motion where the multi-body system is considered as one rigid system (Tysse and Egeland 2018). Later, Cibicik et al. derived the equations of motion for the ship and crane dynamics, where the constraint forces for a crane and a compensation platform were determined and applied to the ship (Cibicik and Egeland 2018; Cibicik et al. 2019). However, it has been noted that hydrodynamic effects of the ship motion response are still challenging for time-domain simulation. In recent years, there is a trend of integrating computational fluid dynamics techniques into such hybrid solutions. These methods are in general time-consuming, which prevents them from wider applications as today (Liu et al. 2014).

In previous work, we presented simulation of offshore crane operation using object-oriented modelling and co-simulation based on the Functional Mock-up Interface (FMI) standard (Chu et al. 2018). The main advantage of this approach is the modularisation of complex dynamic systems for modelling and efficient coupling of domain-specific simulation tools. One of the challenges with co-simulation is the dynamic coupling of tightly coupled systems (Rokseth et al. 2017). For example, a small ship and a deck crane with a heavy payload whose dynamic inertial impacts on the ship cannot be neglected during operation. Tightly coupled systems are not naturally fit to be handled separately for co-simulation. In this very example, the crane and the payload can be connected via a flexible cable and treated as one component. The connection between the ship hull and the crane base can also be represented by a spring-damper system with high stiffness and low damping coefficient. However, it requires extreme high computing resource for real-time simulation which is critical for crane operations in this application. Alternatively, the forces from the crane including the payload can be approximated as external forces and applied to variant attacking points on the ship hull during operation.

CONTACT Yingguang Chu yingguang.chu@sintef.no Sintef Ålesund AS, Borgundvegen 340, 6009 Ålesund, Norway

In this paper, we present coupled simulation of a heavy load crane with ship motion in waves, where the dynamic forces from the crane and payload are applied to the ship. Conservative forces of the crane and payload, i.e. the gravitation forces, are also treated as external forces. Although gravitation forces do not affect the ship's planetary motions, i.e. the surge, sway and yaw motion, but contribute to the heave, pitch and especially, the roll motion. Furthermore, the ship in operation is usually in Dynamic Positioning (DP) control to stabilise these movements. Nevertheless, DP control of the ship is not the focal point of this paper. The heave, pitch and roll motion are usually more critical for such operations, especially the heave and roll motions. Simulation coupling of the ship-crane-load system was tested in the co-simulation platform developed as result of a joint industry project (Smogeli et al. 2020).

The rest of the paper is organised as follows: in Section 2 we describe the kinematics and dynamics of the system and the transformations for coupling the crane and payload to the ship. The simulation results are presented in Section 3, where we discuss the ship motion responses under the impacts of the crane and payload during operation. Finally, in Section 4 the conclusions are drawn.

2. Rigid body motion

2.1. Kinematics and dynamics

The study of kinematics and dynamics of multi-body systems has its heart at the study of motion of rigid objects and their transformation in space. In this paper, we describe the motion of the multi-link crane using the Denavit-Hartenberg (D-H) method (Craig 2009). D-H method is a classic method for analysing the kinematic structure of serial robotic manipulators. A reference frame is attached to each link of a multi-body mechanism such as a robotic arm or a crane. The D-H convention gives a homogeneous transformation matrix ${}^{i-1}_{i}T$ from reference frame $\{i\}$ to reference frame $\{i–1\}$, written as Equation (1). The following four D-H parameters are used: a_{i-1} is the offset distance from $\hat{Z}_{i-1}$ to $\hat{Z}_i$ along $\hat{X}_{i-1}$; α_{i-1} is the offset angle from $\hat{Z}_{i-1}$ to $\hat{Z}_i$ about $\hat{X}_{i-1}$; d_i is the distance from $\hat{X}_{i-1}$ to $\hat{X}_i$ along $\hat{Z}_i$; θ_i is the joint angle from $\hat{X}_{i-1}$ to X_i about Z_i. We use many trigonometric functions in deriving the kinematics and dynamics of the multi-link crane. The notations for sine and cosine in this paper takes the form of $\sin\theta_i = s\theta_i = s_i$ and $\cos\theta_i = c\theta_i = c_i$.

$$ {}^{i-1}_{i}T = \begin{bmatrix} c\theta_i & -s\theta_i & 0 & a_{i-1} \\ s\theta_i c\alpha_{i-1} & c\theta_i c\alpha_{i-1} & -s\alpha_{i-1} & -s\alpha_{i-1}d_i \\ s\theta_i s\alpha_{i-1} & c\theta_i s\alpha_{i-1} & c\alpha_{i-1} & c\alpha_{i-1}d_i \\ 0 & 0 & 0 & 1 \end{bmatrix} \quad (1) $$

The Palfinger crane on the research vessel in Figure 1 consists of three rotational joints and a translational joint. Following the D-H convention, the crane's kinematic structure is described using five reference frames from the base to the tip, as shown in Figure 2. To be noted that the last telescopic link l_3 consists of eight segments. The blue lines represent the simplified line sketch for the links, and each link represents one rigid body of the crane. The green lines represent simplified geometrical relations for the transformation between the crane cylinders and the joints.

The D-H table of the Palfinger crane is given in Table 1 including the default dimensions of the links. Substituting these parameters, the transformation matrix from the crane tip frame to the crane base frame ${}^{0}_{5}T$ can be obtained. The result of ${}^{0}_{5}T$, also called the forward kinematic matrix, is enclosed in the appendix of this paper.

The time derivative of the forward kinematic matrix yields the Jacobian of the manipulator. The Jacobian relates the joint velocities to the Cartesian velocities of the tip of the crane, as shown in Equation (2). Practically, the inverse of Equation (2) gives the required joint velocities by the tip velocities. In the force domain, the Jacobian relates the joint torques that counterbalance the static forces at the tip of the manipulator. Equation (3) shows the mapping of the cartesian forces at the tip of the manipulator to the joint torques by the Jacobian

Figure 1. Offshore crane operation on a research vessel (left), and simulation (right). (This figure is available in colour online.)

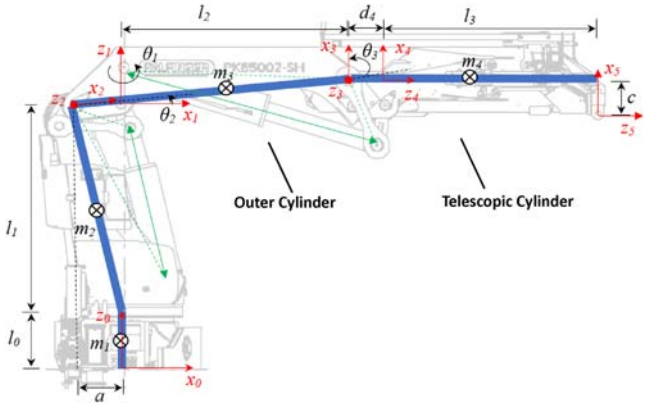

Figure 2. Kinematic reference frames of the Palfinger crane from base to tip according to the Denavit-Hartenberg convention. (This figure is available in colour online.)

Table 1. D-H table.

i	a_{i-1} (m)	α_{i-1} (deg)	d_i (m)	θ_i (deg)
1	0	0°	l_0+l_1(0.2 + 1.8)	θ_1
2	a(0.38)	90°	0	θ_2
3	l_2(1.85)	0°	b(−0.6)	θ_3
4	0	90°	d_4	0°
5	c(−0.5)	0°	l_3(2*8)	0°

Note: b is not shown in Figure 2. It represents the distance between link 2 and link 3, i.e. from axis x_2 to x_3 according to z_3. d_4 is the total displacement of the telescopic joint.

transpose. The results of the Jacobian ${}^0_5J$ of the Palfinger crane is given in the appendix.

$$ {}^0_5\nu = {}^0_5J(\theta)\dot{\theta} \tag{2} $$

$$ \tau = {}^0_5J^{T0}_5F \tag{3} $$

We use the Lagrangian approach to derive the equations of motion for the multi-body crane. Lagrange's equations provide an elegant formulation of the dynamics of a mechanical system. It reduces the equations needed to describe the motion of the system using generalised coordinates instead of every single body with mass and inertia. It also provides a convenient form for modelling using the energy-based method, namely, the Bond Graph method (Chu and Æsøy 2015; Karnopp et al. 2012). The Lagrangian L is defined as the difference between the kinetic energy K and the potential energy V of the system, as given by Equation (4).

$$ L(\theta, \dot{\theta}) = K(\theta, \dot{\theta}) - V(\theta) = \frac{1}{2}\dot{\theta}^T M(\theta)\dot{\theta} - V(\theta) \tag{4} $$

where $M(\theta)$ is the manipulator inertia matrix.

The equations of motion can be obtained by substituting Equation (4) into the Lagrange's equations:

$$ \frac{d}{dt}\frac{\partial L}{\partial \dot{\theta}} - \frac{\partial L}{\partial \theta} = Y \tag{5} $$

where Υ represents the actuation forces (torques) and other nonconservative forces (torques), or generalised forces acting on the joints.

To apply Lagrange's equations to the multi-body crane, we must calculate its kinetic and potential energy. The kinetic energy of the ith link is given by:

$$ K_i = \frac{1}{2}m_i v_i^T v_i + \frac{1}{2}\omega_i^T I_i \omega_i = \frac{1}{2}V_i^T M_i V_i = \frac{1}{2}\dot{\theta}^T J_i^T M_i(\theta) J_i \dot{\theta} \tag{6} $$

where v_i denotes the body velocity and J_i is the body Jacobian corresponding to the centre of mass of the ith link.

The total kinetic energy can be written in the generalised form as below:

$$ K(\theta, \dot{\theta}) = \frac{1}{2}\dot{\theta}^T M(\theta)\dot{\theta} \tag{7} $$

The generalised inertia matrix $M(\theta)$ can be obtained by:

$$ M(\theta) = \sum_{i=1}^{n} J_i^T(\theta) M_i J_i(\theta) \tag{8} $$

Using Equations (4) and (5) we have

$$ \frac{d}{dt}\frac{\partial L}{\partial \dot{\theta}} = \frac{d}{dt}\left(\sum_{j=1}^{n} M_{ij}\dot{\theta}_j\right) = \sum_{j=1}^{n}\left(M_{ij}\ddot{\theta}_j + \dot{M}_{ij}\dot{\theta}_j\right) \tag{9} $$

$$ \frac{\partial L}{\partial \theta} = \frac{1}{2}\sum_{j,k=1}^{n}\frac{\partial M_{kj}}{\partial \theta_i}\dot{\theta}_k\dot{\theta}_j - \frac{\partial V}{\partial \theta_i} \tag{10} $$

Expanding the $\dot{M}_{ij}$ term in terms of partial derivatives and rearranging the equation, we can get:

$$ \sum_{j=1}^{n} M_{ij}\ddot{\theta}_j + \sum_{j,k=1}^{n}\Gamma_{ijk}\dot{\theta}_j\dot{\theta}_k + \frac{\partial V}{\partial \theta_i} = \Upsilon_i \quad i = 1, \ldots, n \tag{11} $$

where Γ_{ijk} is given by:

$$ \Gamma_{ijk} = \frac{1}{2}\left(\frac{\partial \mathrm{M}_{ij}}{\partial \theta_k} + \frac{\partial \mathrm{M}_{ik}}{\partial \theta_j} - \frac{\partial \mathrm{M}_{kj}}{\partial \theta_i}\right) \tag{12} $$

The centrifugal and Coriolis terms in Equation (11) arise because of the non-inertial frames, which are implicit in the use of generalised coordinates. We use the functions Γ_{ijk}, so-called Christoffel symbols to write the C_{ij} matrix corresponding to the inertia matrix $M(\theta)$. To put the equations of motion back into vector form, the Coriolis matrix $C(\theta, \dot{\theta})$ is written as:

$$ C_{ij}(\theta, \dot{\theta}) = \sum_{k=1}^{n}\Gamma_{ijk}\dot{\theta}_k = \frac{1}{2}\left(\frac{\partial \mathrm{M}_{ij}}{\partial \theta_k} + \frac{\partial \mathrm{M}_{ik}}{\partial \theta_j} - \frac{\partial \mathrm{M}_{kj}}{\partial \theta_i}\right)\dot{\theta}_k \tag{13} $$

Finally, the potential energy of the ith link is:

$$ V_i = -m_i g h_i \tag{14} $$

where h_i represents the height of the centre of gravity of the ith link.

The external forces can be divided into two components. Let τ represent the force applied at the joint and define $N(\theta, \dot{\theta})$ as other forces including the conservative forces and frictional forces.

$$ N(\theta, \dot{\theta}) = \frac{\partial V}{\partial \theta} + \beta\dot{\theta} \tag{15} $$

This completes the derivation of the dynamics of the crane, as given by Equation (16). The M and C matrices of the Palfinger crane are enclosed in the appendix.

$$ M(\theta)\ddot{\theta} + C(\theta, \dot{\theta})\dot{\theta} + N(\theta, \dot{\theta}) = \tau \tag{16} $$

2.2. The ship model in waves

The ship model in waves is in six degree of freedom (6-DoF) with DP control. It is based on Fossen's unified nonlinear model for ship-like structures subjected to waves, wind and currents (Fossen 2005). The ship is a 6-DoF rigid body moving object where the fluid effect memories are modelled in a state space form. It combines the manoeuvring and seakeeping ship models in a single code solved by Sintef's time-domain simulator VeSim (Hassani et al. 2015). The equation of motion of the ship is given by Equation (17).

$$ M\dot{\nu} + C(\nu)\nu + D(\nu)\nu + g(\eta) + g_0 = \tau \tag{17} $$

where ν and η represent the vectors of generalised velocities and positions of the ship. τ is the generalised external forces including the environmental forces, the propulsion thrust forces and other external forces such as the applied forces from the crane and payload. The inertia matrix M consists of the rigid body mass and added mass. $C(\nu)$ and $D(\nu)$ denotes the Coriolis-centripetal and damping forces and

moments, respectively. $g(\eta)$ describes the restoring force term. Static restoring forces and moments due to ballast systems and water tanks are collected in the term g_0.

In VeSim, the hydrodynamic properties of the ship are calculated in advance using Sintef's strip-theory code ShipX, Vessel Responses (VERES), and the manoeuvring coefficients are calculated using the semi-empirical code ShipX Manoeuvring Plug-In (HullVisc). A series of complex manipulations and corrections must be done carefully to get a combined manoeuvring and seakeeping ship model, because some effects may appear twice in both the manoeuvring and seakeeping formulations. Simply speaking, these effects include the restoring forces in low-frequency motions added-mass and Coriolis-centripetal forces in wave frequency motions, and the damping forces and moments. In order to validate the ship model, a set of model test experiments were carried out on a scaled prototype of the Gunnerus ship. These include resistance tests, propulsion tests and Planar Motion Mechanism (PMM) tests. Full scale sea trials on the Gunnerus ship were also conducted and the data were used to tune the simulation model. For more details of the VeSim simulator and model tests, see Hassani et al. (2015) and relevant references.

2.3. Transformations

In order to couple the ship-crane-load together, transformations for the motions of the objects and reaction forces are needed. The transformation between the ship and the crane including the payload is given by the surge-sway-heave motions and roll-pitch-yaw Euler angles $\psi,\ \theta,\ \varphi$, as shown in Figure 3. Equation (18) gives the linear velocity transformation from the body frame to the global frame. Similarly, Equation (19) gives the generalised linear force transformation. The superscript and subscript in the equations represents the mapping between the reference frames of the system. More specifically, from the crane tip to the crane base {0}, to the Centre of Gravity (CoG) of the ship and the global frame {g}.

$$v^g_{\text{tip}} = v^g_{\text{ship}} + R(\psi,\ \theta,\ \varphi)v^{\text{CoG}}_{\text{tip}} \tag{18}$$

$$F^g_{\text{ship}} = F^g_{\text{tip}} - \sum G^g_i \tag{19}$$

where G^g_i denotes the gravitation force of the crane's ith link. The negative sign here represents the direction of the forces.

The rotation matrix $R(\psi,\ \theta,\ \varphi)$ from frame $\{i\}$ to the ship frame attached to the CoG of the ship is given by Equation (20):

$$R(\psi,\ \theta,\ \varphi) = \begin{bmatrix} c\psi c\theta & c\psi s\theta s\varphi - s\psi c\varphi & c\psi s\theta c\varphi + s\psi s\varphi \\ s\psi c\theta & s\psi s\theta s\varphi + c\psi c\varphi & s\psi s\theta c\varphi - c\psi s\varphi \\ -s\theta & c\theta s\varphi & c\theta c\varphi \end{bmatrix} \tag{20}$$

The payload is modelled as a freely suspended pendulum attached to the crane tip by a segment of wire. The wire model is a linear spring-damper simplification. Figure 4 shows the reference frames for deriving the transformation between the payload and the crane tip.

The force vector F_{tip} applied on the crane tip can be obtained from the wire tension F_{wire}. The minus sign indicates the direction of the forces.

$$F_{\text{tip}} = -\begin{bmatrix} \frac{\Delta x}{l} & \frac{\Delta y}{l} & \frac{\Delta z}{l} \end{bmatrix}^T$$

$$F_{\text{wire}} = -\begin{bmatrix} \frac{\Delta x}{\sqrt{\Delta x^2 + \Delta y^2 + \Delta z^2}} & \frac{\Delta y}{\sqrt{\Delta x^2 + \Delta y^2 + \Delta z^2}} \\ \frac{\Delta z}{\sqrt{\Delta x^2 + \Delta y^2 + \Delta z^2}} & \end{bmatrix}^T F_{\text{wire}} \tag{21}$$

Finally, the Jacobian transpose from the crane tip forces to the joint torques complete the transformation.

$$\tau = {}^0_5J(\theta)^T\ F^0_{\text{tip}} \tag{22}$$

3. Simulation results

Simulation coupling of the ship-crane-load system was tested in the open simulation platform (Smogeli et al. 2020). We would like to highlight the use of distributed simulation enabled by FMU-proxy. FMU-proxy is an open, language- and platform-independent co-simulation

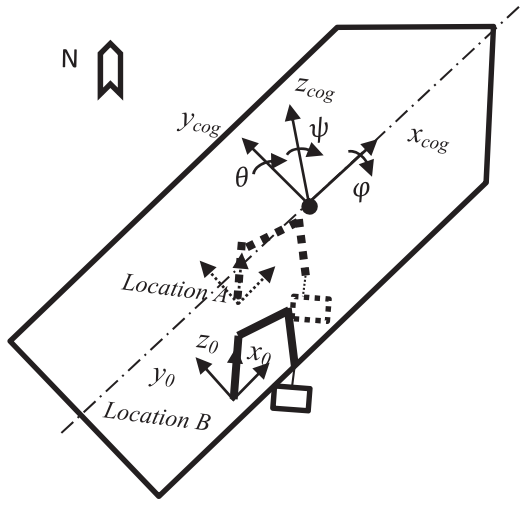

Figure 3. Reference frames from ship to crane base.

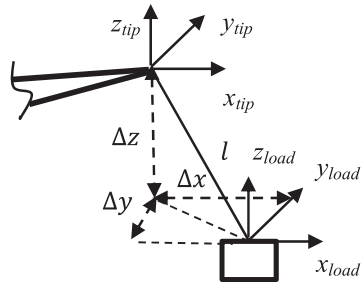

Figure 4. Reference frames of the suspended load to the crane tip.

platform based on the FMI standard (Hatledal et al. 2019). Distributed simulation provides an alternative solution to accommodate certain use cases, such as overcoming licence and software requirements, access from unsupported platforms or languages and safe invocation of an FMU by running it in a sand-boxed environment. In this section, we show the results of the ship motion response under the external forces from the crane and load. In the simulation cases, the Gunnerus ship model is 33.9 m length between perpendiculars, 9.6 m breadth and 107 tons dead weight. The crane has a total weight of 5.9 tons with a payload of 700 kg. In the test cases, the DP controller is activated at 50 s from the start of the simulation. Since the DP controller is not ideal, it contributes to the ship motions. Figure 5 shows the performance of the DP control with the crane installed at Location B on the ship. As can be seen, the ship motions are kept relatively stable after 200 s in the given environmental conditions. Although DP control is not the focal point of this paper, we have crane operations start after the ship motions are relatively stable as in real world operations.

3.1. Case 1: Crane with lifted payload at different locations on deck

An offshore crane usually operates on the port side or starboard side of the ship. Regardless of the weight distribution and ballasting of the ship, a crane with a heavy load on either side of the ship affects the ship response significantly, especially the roll motion. Figure 6 shows the roll angle of the ship with the crane at Location A and Location B. The position vectors of the ship's CoG, Location A and Location B are

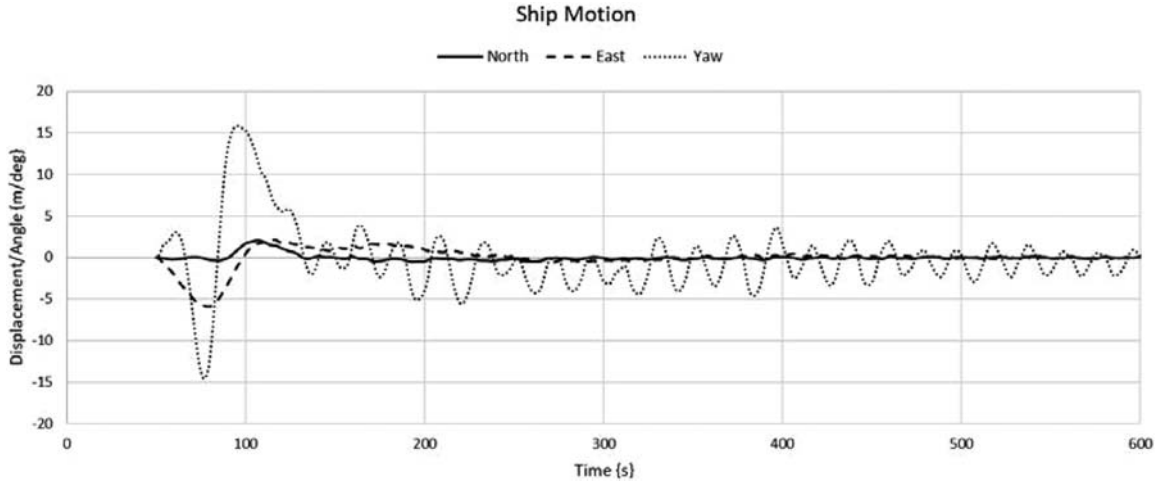

Figure 5. Ship motion with the crane at Location B. Environmental conditions are: wave height 0.3 m, wave period 10 s; current velocity 0.5 m/s; wind velocity 1 m/s; wave, current and wind velocity direction −135°N.

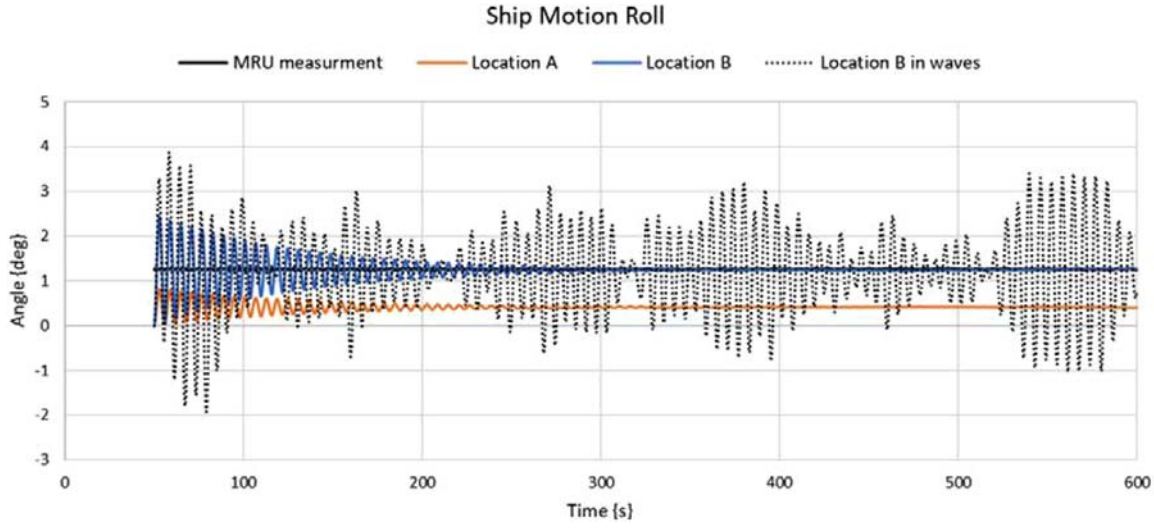

Figure 6. Ship motion with the crane at different locations in calm water conditions and in waves. Environmental conditions: wave height 0.3 m, wave period 10 s; current velocity 0.5 m/s; wind velocity 1 m/s; wave, current and wind velocity direction −135°N. (This figure is available in colour online.)

given in Equation (23) relative to the aft perpendicular, centre line and baseline of the ship.

$$\begin{aligned} P_{\text{cog}} &= \begin{bmatrix} 15.516 & 0 & 3.624 \end{bmatrix}^T, P_A \\ &= \begin{bmatrix} 10.516 & -1 & 6.624 \end{bmatrix}^T, P_B \\ &= \begin{bmatrix} 5.516 & -3 & 6.624 \end{bmatrix}^T \end{aligned} \tag{23}$$

The MRU measurement shows the ship angle in calm water condition for comparison. Location B is where the crane is installed on the real vessel. The roll angle eventually stabilised to the same level as the MRU measurement depending on the environmental conditions. Location A is closer to the CoG of the ship than Location B. As can be seen from the simulation results, the average roll angle of the ship becomes smaller when the crane is placed at Location A than at Location B.

3.2. Case 2: Crane lifting operation in calm water

The lifting scenario is defined as illustrated in Figure 7. We divide the whole operation into five steps. The initial state of the system is with the crane at the starboard side of the ship, i.e. Location B in Figure 3, with the outer boom extended over the payload.

The roll response of the ship reflects the disturbances from the crane movement, as shown in Figure 8. The roll motion is excited at 50 s when the external forces applied including the thruster forces and the crane forces. The ship gradually restores its position and balance after 200 s. Crane lifting operation starts from 220 s following the procedure in Figure 8. The crane main boom and slewing joint angles are shown in Figure 9. Small variations can be seen from the ship roll response as the main boom lifts and lowers the payload at 220 and 300 s, respectively. The ship roll angle decreases as the slewing joint of the crane moves from starboard side to port side.

3.3. Case 3: Crane lifting operation in waves

In the third test case, we present simulation of the crane operation in waves. It is necessary and useful to find out potential risks for operation and allowed weather window to conduct the operation. Figure 10 shows the roll response of the ship when the crane operates as described in test case 2. As can be seen, the roll angle increased significantly comparing to case 2 in calm water. The ship motions cause large movements of the crane and the payload, as shown in Figure 11. As a result, large dynamic forces from the crane and payload are generated. The movements of the ship in such conditions are challenging for safe operation with a heavy load. Therefore, it is advised to start crane operation in better conditions. The load follows the crane tip movements with minimal relative offsets. The initial wire length is 1 m, which is a short segment considering the crane movement range. As a result, it shows small load swing relative to the crane tip positions in north and east direction. Load swing can increase significantly when the wire is released via the winch system. It would be challenging to manoeuvre the crane with a heavy load safely at such conditions without compensation.

4. Conclusions

In this paper, we presented coupled simulation of crane operation and ship response in waves. We utilised the co-simulation approach presented in earlier work, where the simulation of the ship model in waves and the crane with payload are handled separately. The co-simulation approach enables the use of different domain software tools for complex multi-domain systems. It also improves the simulation

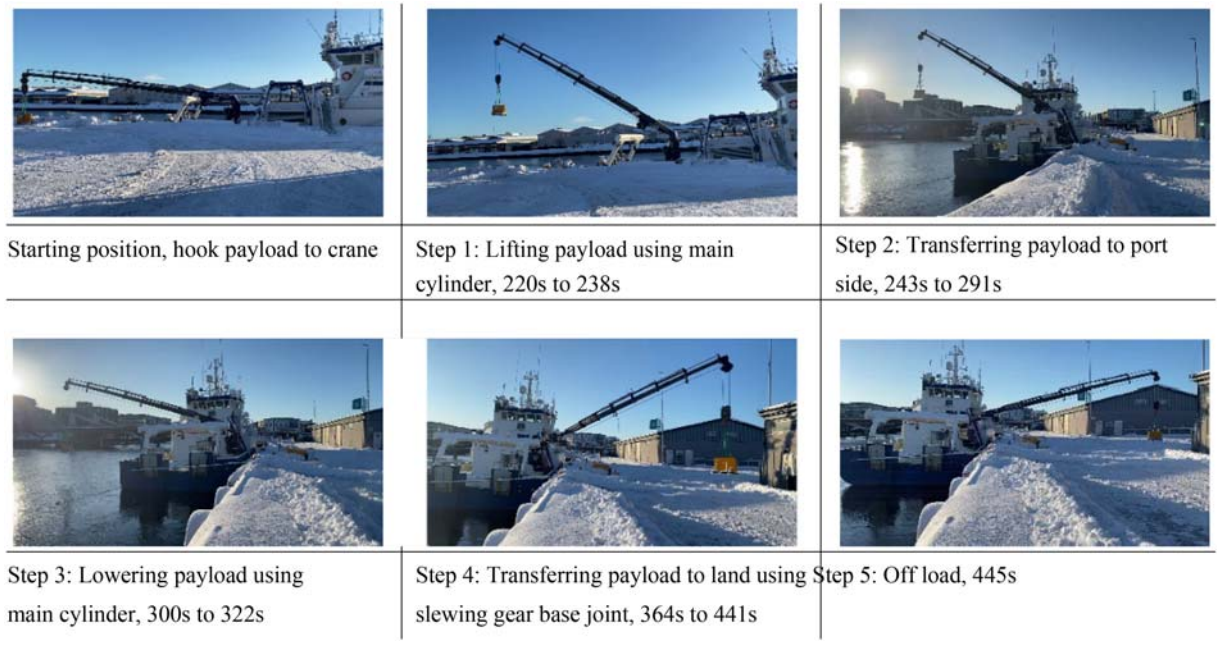

Figure 7. Crane lifting operation scenario. (This figure is available in colour online.)

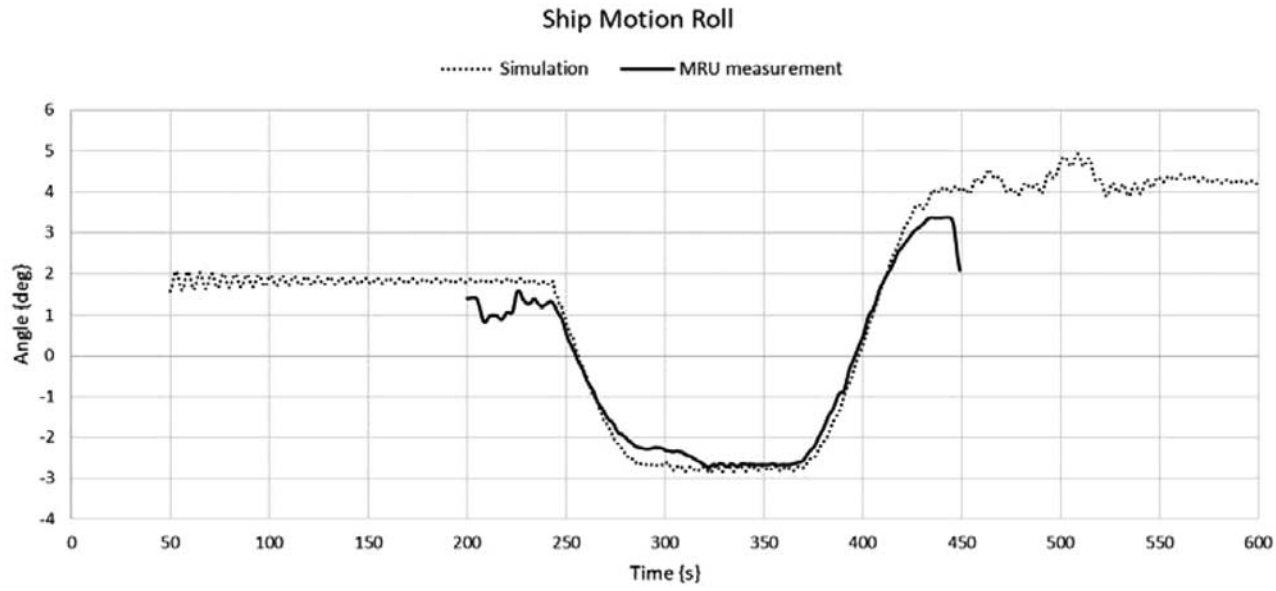

Figure 8. Roll angle of the ship during crane operation in calm water.

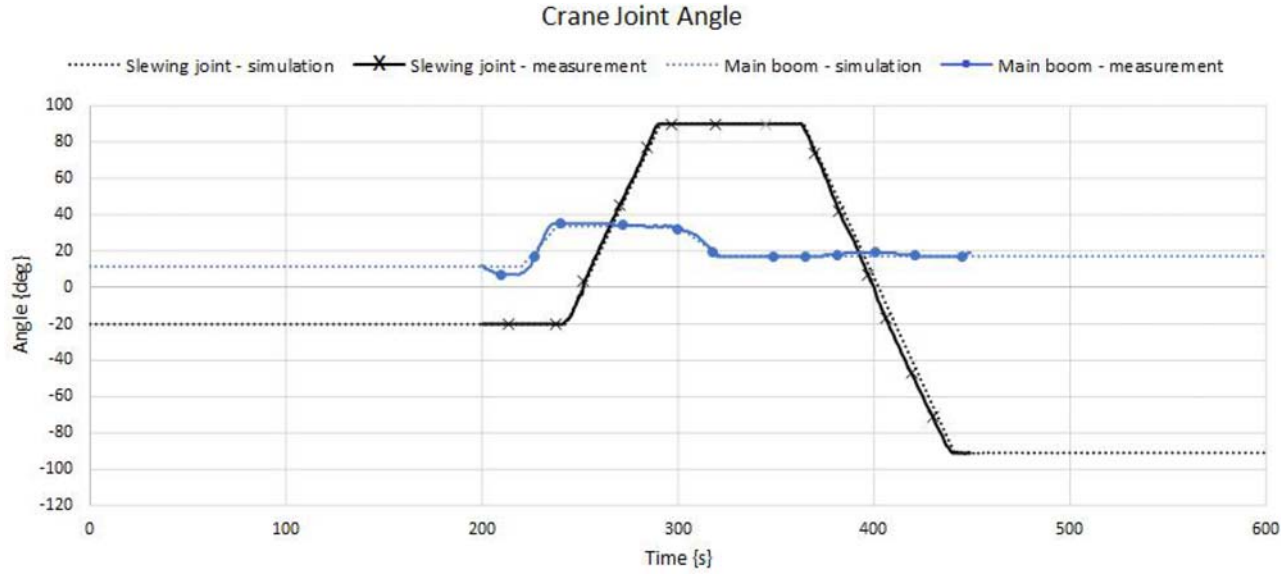

Figure 9. Crane joint angles during crane operation in calm water. (This figure is available in colour online.)

efficiency through the orchestration of the sub-simulators and parallel computation using multiple processes. It depends on the application to determine the acceptable co-simulation time steps and numerical errors. For the system presented in the test cases, the real time index is about 30, meaning that the simulation time is about 1/30 of the clock time.

The derivation of the kinematics and dynamics of the system was described. The transformations and equations of motion of the multi-body system were established using the D-H method and the Lagrangian approach. It provides a systematic procedure to describe rigid body motions in space and is widely applied in robotics. Other methods were not discussed, but mentioned here as a good alternative, is the screw theory (Murray et al. 1994). The simulation results of three test cases were discussed to demonstrate the impacts of a heavy lifting crane operation to the ship motions. Case 1 shows the roll response of the ship when the crane is installed in difference deck locations. A heavy lifting crane can significantly affect the ship weight distribution, hence its motion response. There are usually balancing solutions on board for onboard weight distribution, and for moving equipment, for example, through ballasting during operation. Case 2 and 3 show the results of the ship response during crane lifting operation. It can be seen the crane system has large impacts on the ship motion as the payload is transferred. In return, the ship motion causes large deviations to the crane and payload positions. Other onboard equipment was not taken into consideration in simulation, which also contributes to the overall

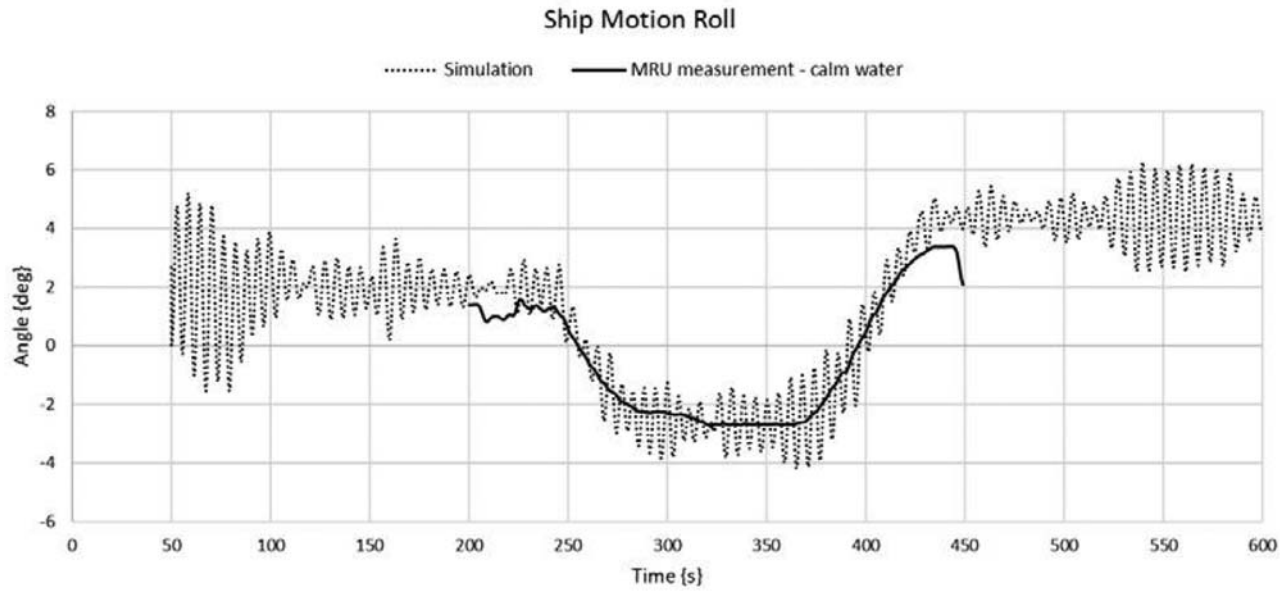

Figure 10. Roll angle of the ship during crane operation in waves. Environmental conditions are: wave height 0.5 m, wave period 10 s; current velocity 1 m/s; wind velocity 3 m/s; wave, current and wind velocity direction −135°N.

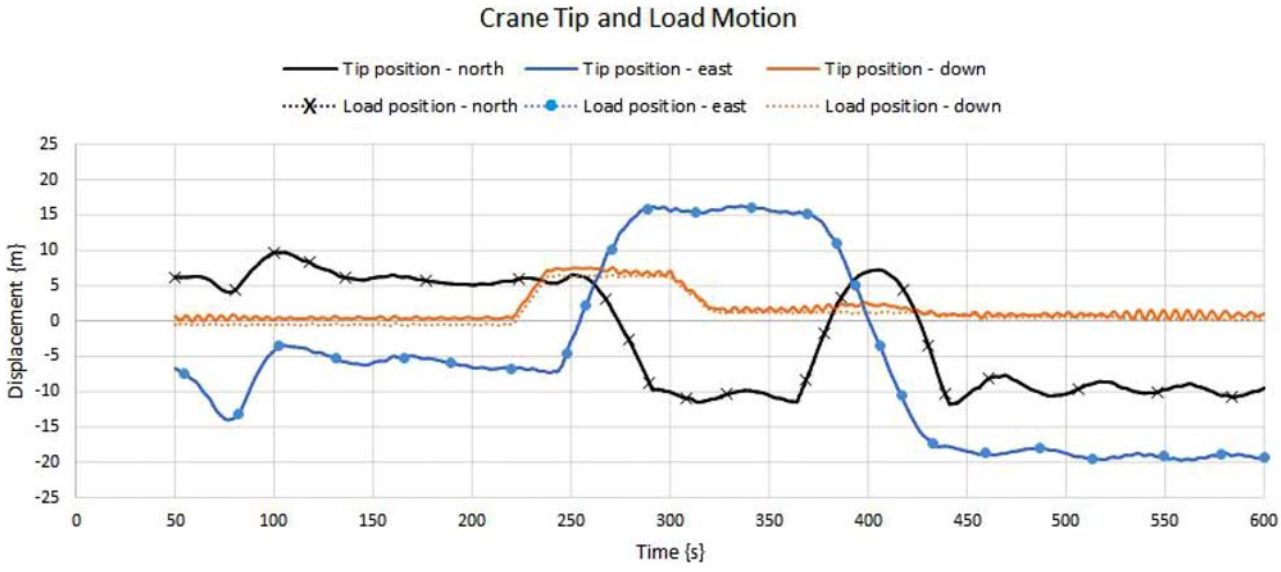

Figure 11. Crane tip position and payload position during crane operation in waves. Environmental conditions are: wave height 0.3 m, wave period 10 s; current velocity 0.5 m/s; wind velocity 1 m/s; wave, current and wind velocity direction −135°N. (This figure is available in colour online.)

weight distribution. The testing data are thus only to demonstrate the effectiveness of the proposed approach and validate the simulation results. It requires extensive tests, both in a towing tank and through sea trails, to tune the ship model. This is out of the scope of this project.

The co-simulation approach offers an efficient way for real-time simulation of complex multi-domain systems, however, the challenges regarding tightly coupled systems remain. Establishing the equations of motion of the ship alone has been done, while having a running model with tightly coupled system in real time is non-trivial. Like the wave excitation forces, the forces from the crane and payload were treated as external forces applied on the right-hand of the equations of motion in the ship model. These external forces are applied at different attack points on the ship hull, i.e. the CoG of the crane and the crane tip position for the load forces. Other alternative approaches to obtain the ship motion in waves can utilise data-driven techniques instead of model-based methods. In Li et al. (2017), a data-driven model for time series prediction of ship motion is presented. However, the performance of data-driven methods is dependent on the obtained data set for training and prediction. Such data in the maritime domain is often limited. Moreover, the accuracy of longer time prediction is another challenge for demanding operations such as crane heavy lifting. It is shown that predictions, in most cases, can be made fairly accurate up to 20 s ahead of

the current time (Nielsen and Jensen 2017). Accurate longer time predictions cannot be improved by measured motion sensor data alone. Methods using both weather forecast and wave buoys to predict sea states can be combined with the ship motion data to extend the prediction period and reduce the error. This calls for an efficient solution for model tuning of the ship response model in waves, specifically, the M, $C(v)$ and $D(v)$ matrices and the restoring forces in Equation (17).

Acknowledgements

Special thanks go to Sintef Ocean for their efforts on the reference models in the Open Simulation Platform project.

Disclosure statement

No potential conflict of interest was reported by the author(s).

Funding

The project is financially supported by the funding from the Research Council of Norway (Norges Forskningsråd) with MAROFF KPN 'Digital Twins for Vessel Life Cycle Service', project no. 280703, and partly by a grant from EU H2020 (Horizon 2020) project 'Arrowhead Tools for Engineering of Digitalisation Solutions', project no. 826452.

ORCID

Yingguang Chu http://orcid.org/0000-0002-1504-6891
Guoyuan Li http://orcid.org/0000-0001-7553-0899
Houxiang Zhang http://orcid.org/0000-0003-0122-0964

References

Baar JJM, Pijfers JGL, van Santen JA. 1992. Hydromechanically coupled motions of a crane vessel and a transport barge. Proceedings of Offshore Technology Conference; May 4–7; Houston, USA. p. 127–136.

Chu Y, Æsøy V. 2015. A multi-body dynamic model based on bond graph for maritime hydraulic crane operations. ASME 2015 34th International Conference on Ocean, Offshore and Arctic Engineering; May 31–Jun 5; St. John's, Newfoundland, Canada. p. OMAE2015-41616, V001T01A010.

Chu Y, Hatledal LI, Æsøy V, Ehlers S, Zhang H. 2018. An object-oriented modeling approach to virtual prototyping of marine operation systems based on functional mock-up interface co-simulation. J Offshore Mech Arct Eng. 140:2.

Cibicik A, Egeland O. 2018. Determination of constraint forces for an offshore crane on a moving base. 2018 5th International Conference on Control, Decision and Information Technologies (CoDIT); Apr 10–13; Thessaloniki, Greece. p. 233–240.

Cibicik A, Tysse GO, Egeland O. 2019. Determination of reaction forces of a deck crane in wave motion using screw theory. J Offshore Mech Arct Eng. 141:6.

Craig JJ. 2009. Introduction to robotics: mechanics and control, 3/E. Upper Saddle River, NJ: Pearson Education Inc.

Fossen TI. 2005. A nonlinear unified state-space model for ship maneuvering and control in a seaway. Int J Bifurcation Chaos. 15 (09):2717–2746.

Hassani V, Ross A, Selvik Ø, Fathi D, Sprenger F, Berg TE. 2015. Time domain simulation model for research vessel Gunnerus. 34th International Conference on Ocean, Offshore and Arctic Engineering; St. John's, Newfoundland, Canada, OMAE2015-41786, 2015. St. John's, Newfoundland, Canada.

Hatledal LI, Styve A, Hovland G, Zhang H. 2019. A language and platform independent co-simulation framework based on the functional mock-Up interface. IEEE Access. 7:109328–109339.

Karnopp DC, Margolis DL, Rosenberg RC. 2012. System dynamics: modeling, simulation, and control of mechatronic systems, 5th ed. Hoboken: John Wiley.

Li G, Kawan B, Wang H, Zhang H. 2017. Neural-network-based modelling and analysis for time series prediction of ship motion. Ship Technol Res. 64(1):30–39.

Liu S, Papanikolaou A, Zaraphonitis G. 2014. Time domain simulation of nonlinear ship motions using an impulse response function method. Proceedings of the International Conference on Maritime Technology ICMT; Jul 7–9; Glasgow, UK.

Murray RM, Li Z, Sastry SS, Sastry SS. 1994. A mathematical introduction to robotic manipulation. Boca Raton, FL: CRC press.

Nielsen UD, Jensen JJ. 2017. Deterministic predictions of vessel responses based on past measurements. Proceedings of the 27th International Ocean and Polar Engineering Conference; Jun 25–30; San Francisco, California, USA. p. 513–518.

Rokseth B, Skjong S, Pedersen E. 2017. Modeling of generic offshore vessel in crane operations with focus on strong rigid body connections. IEEE J Oceanic Eng. 42(4):846–868.

Schellin T, Jiang T, Sharma S. 1991. Crane ship response to wave groups. J Offshore Mech Arct Eng. 113(3):211–218.

Smogeli Ø, Vik B, Nordahl H, Kyllingstad LT, Zhang H. 2020. Open simulation platform: an ecosystem for digital twin system simulations. Proceeding of 19th Conference on Computer and IT Applications in the Maritime Industries COMPIT'20; May 11–13; Pontignano, Italy. p. 239–253.

Tysse GO, Egeland O. 2018. Dynamic interaction of a heavy crane and a ship in wave motion. Model. Identif. Control: Nor. Res. Bull. 39(2):45–60.

Appendix

Derivation of the kinematics and dynamics of the Palfinger crane

The transformation matrix from the crane tip frame {5} to the crane base frame {0} is given by:

$$
{}^0_5T = \begin{bmatrix} {}^0_5\boldsymbol{R} & {}^0_5\boldsymbol{P} \\ 0 & 1 \end{bmatrix}
= \begin{bmatrix} & c_1(-a + cc23 + l_2c_2 + (l_3 + d_4)s_{23}) + bs1 \\ {}^0_5\boldsymbol{R} & s_1(-a + cc23 + l_2c_2 + (l_3 + d_4)s_{23}) - bc1 \\ & l_0 + l_1 + cs_{23} + l_2s_2 - (l_3 + d_4)c_{23} \\ \boldsymbol{0} & \boldsymbol{1} \end{bmatrix}
$$

The Jacobian matrix can be obtained from the position vector ${}^0_5\boldsymbol{P}$:

$$
{}^0_5J = \begin{bmatrix} -s_1(-a + cc23 + l_2c_2 + (l_3 + d_4)s_{23}) + bc1 & c_1(-l_2s_2 + (l_3 + d_4)c_{23} + cs23) & c_1((l_3 + d_4)c_{23} - cs23) & c_1s_{23} \\ c_1(-a + cc23 + l_2c_2 + (l_3 + d_4)s_{23}) + bs1 & s_1(-l_2s_2 + (l_3 + d_4)c_{23} + cs23) & s_1((l_3 + d_4)c_{23} - cs23) & s_1s_{23} \\ 0 & l_2c_2 + (l_3 + d_4)s_{23} + cc23 & (l_3 + d_4)s_{23} + cc23 & -c_{23} \end{bmatrix}
$$

The non-zero elements of the inertia matrix $M(\theta)$ are given as follows:

$$M(\theta) = \begin{bmatrix} M_{11} & M_{12} & M_{13} & M_{14} \\ M_{21} & M_{22} & M_{23} & M_{24} \\ M_{31} & M_{32} & M_{33} & M_{34} \\ M_{41} & M_{42} & M_{43} & M_{44} \end{bmatrix}$$

$$\begin{aligned} M_{11} = {} & I_{y2}*s_2^2 + I_{y3}*s_{23}^2 + I_{y4}*s_{23}^2 + +I_{z1} + I_{z2}*c_2^2 + I_{z3}*c_{23}^2 + I_{z4}*c_{23}^2 \\ & + m_2*r_1^2*c_2^2 + m_3*(l_1*c_2 + r_2*c_{23})^2 \\ & + m_4*(l_1*c_2 + (r_3 + d_4)*c_{23})^2 \end{aligned}$$

$$\begin{aligned} M_{22} = {} & I_{x2} + I_{x3} + I_{x4} + m_3*l_1^2 + m_4*l_1^2 + m_2*r_1^2 + m_3*r_2^2 \\ & + m_4*(r_3 + d_4)^2 + 2*m_3*l_1*r_2*c_3 + 2*m_4*l_1*(r_3 + d_4)*c_3 \end{aligned}$$

$$\begin{aligned} M_{23} = {} & I_{x3} + I_{x4} + m_3*r_2^2 + m_4*(r_3 + d_4)^2 + m_3*l_1*r_2*c_3 \\ & + m_4*l_1*(r_3 + d_4)*c_3 \end{aligned}$$

$$M_{24} = I_{x4} + m_4*(r_3 + d_4)^2 + m_4*l_1*(r_3 + d_4)*c_3$$

$$M_{32} = M_{23}$$

$$M_{33} = I_{x3} + I_{x4} + m_3*r_2^2 + m_4*(r_3 + d_4)^2$$

$$M_{34} = I_{x4} + m_4*(r_3 + d_4)^2$$

$$M_{42} = M_{24}$$

$$M_{43} = M_{34}$$

$$M_{44} = M_{43} = M_{34}$$

The non-zero elements of Γ_{ijk} for writing the Coriolis matrix $C(\theta, \dot{\theta})$ are given as follows:

$$C(\theta, \dot{\theta}) = \begin{bmatrix} C_{11} & C_{12} & C_{13} & C_{14} \\ C_{21} & C_{22} & C_{23} & C_{24} \\ C_{31} & C_{32} & C_{33} & C_{34} \\ C_{41} & C_{42} & C_{43} & C_{44} \end{bmatrix}$$

$$\begin{aligned} \Gamma_{112} = {} & (I_{y2} - I_{z2} - m_2*r_1^2)*c_2*s_2 + (I_{y3} - I_{z3} + I_{y4} - I_{z4})*c_{23}*s_{23} \\ & - m_3*(l_1*c_2 + r_2*c_{23})*(l_1*s_2 + r_2*s_{23}) \\ & - m_4*(l_1*c_2 + (r_3 + d_4)*c_{23})*(l_1*s_2 + (r_3 + d_4)*s_{23}) \end{aligned}$$

$$\begin{aligned} \Gamma_{113} = {} & (I_{y3} - I_{z3} + I_{y4} - I_{z4})*c_{23}*s_{23} - m_3*r_2*s_{23}*(l_1*c_2 + r_2*c_{23}) \\ & - m_4*(r_3 + d_4)*s_{23}*(l_1*c_2 + (r_3 + d_4)*c_{23}) \end{aligned}$$

$$\Gamma_{121} = \Gamma_{112}$$

$$\Gamma_{131} = \Gamma_{113}$$

$$\Gamma_{211} = -\Gamma_{121} = -\Gamma_{112}$$

$$\Gamma_{223} = -m_3*l_1*r_2*s_3 - m_4*l_1*(r_3 + d_4)*s_3$$

$$\Gamma_{232} = \Gamma_{223}$$

$$\Gamma_{233} = \Gamma_{232} = \Gamma_{223}$$

$$\Gamma_{311} = -\Gamma_{131} = -\Gamma_{113}$$

$$\Gamma_{322} = -\Gamma_{233} = -\Gamma_{232} = -\Gamma_{223}$$

$$\Gamma_{141} = m_4*(l_1*c_2 + (r_3 + d_4)*c_{23})*c_{23}$$

$$\Gamma_{242} = m_4*(r_3 + d_4) + m_4*l_1*d_4*c_3$$

$$\Gamma_{243} = m_4*(r_3 + d_4) + \frac{1}{2}*m_4*l_1*d_4*c_3 - \frac{1}{2}*l_1*(r_3 + d_4)*c_3*s_3$$

$$\Gamma_{244} = 2*\Gamma_{242}$$

$$\Gamma_{342} = m_4*(r_3 + d_4) + \frac{1}{2}*m_4*l_1*d_4*c_3 + \frac{1}{2}*l_1*(r_3 + d_4)*c_3*s_3$$

$$\Gamma_{343} = m_4*(r_3 + d_4)$$

$$\Gamma_{344} = 2*\Gamma_{343}$$

$$\Gamma_{444} = \Gamma_{343}$$

$$\Gamma_{411} = -\Gamma_{141}$$

$$\Gamma_{422} = -\Gamma_{242}$$

$$\Gamma_{423} = -\Gamma_{444} = -\Gamma_{343}$$

$$\Gamma_{424} = \Gamma_{423}$$

$$\Gamma_{432} = -\Gamma_{342}$$

$$\Gamma_{433} = \Gamma_{423} = -\Gamma_{444} = -\Gamma_{343}$$